A Thermo-Chemo-Mechanical Model for Concrete. II: Damage and Creep

Miguel Cervera,[*] Javier Oliver[†] and Tomás Prato[‡]

ABSTRACT

In this work a coupled thermo-chemo-mechanical model for the behaviour of concrete at early ages is proposed. In this second part the formulation and assessment of the mechanical aspects of the model are presented. The short and long term mechanical behaviour is modelled via a viscoelastic damage model which accounts for the aging effects. The short term model is based on the framework of the Continuum Damage Mechanics Theory. A novel normalized format of the damage model is proposed, so that the phenomenon of aging is accounted for in a natural fashion. Long term effects are included by incorporating a creep model inspired in the Microprestress-Solidification Theory.

[*]Asst. Prof. Struc. Anal., ETS Ingenieros de Caminos, 08034 Barcelona, Spain.
[†]Prof. Cont. Mech., ETS Ingenieros de Caminos, 08034 Barcelona, Spain.
[‡]Grad. Res. Asst., ETS Ingenieros de Caminos, 08034 Barcelona, Spain.

INTRODUCTION

In the companion paper (Cervera et al. 1998) the formulation and assessment of the thermo-chemical aspects of the proposed model were presented. This second part presents the full thermo-chemo-mechanical model which considers many of the relevant features of the mechanical behaviour of concrete at early ages, in a format suitable for its implementation in the general framework of the Finite Element Method. Firstly, a thermo-chemo-mechanical model is proposed to describe the short term behaviour of concrete at early ages. The reference model is based on the theory of Continuum Damage Mechanics and it incorporates two separate scalar internal variables to represent damage both under tension and compression conditions. The damage model is reformulated in a suitable normalized format so that it can incorporate the phenomenon of aging. Secondly, the proposed model is extended to include the long term mechanical behaviour. This is done by incorporating a creep model inspired in the recently proposed Microprestress-Solidification Theory and coupling it to the aging-damage model proposed in the first part of the paper. Finally, different available experimental data sets are used to compare the observed behaviour of conventional and high-performance concrete mixes at early ages with the simulations obtained using the proposed model.

SHORT TERM MECHANICAL BEHAVIOUR

The mechanical behaviour of concrete, like other geomaterials, is complex and highly nonlinear, even for moderate stress levels. A reasonable model should contemplate features such as: (a) large difference in the tensile and compressive strengths, leading to rather distinct stress-strain curves obtained under tension or compression, (b) stiffness recovery upon load sign reversal, that is, passing from tension to compression, or viceversa, (c) strength enhancement under 2D or 3D stress states, when compared to uniaxial tests, (d) plastic deformation after unloading, (e) rate sensitivity, etc. The available literature includes models based on the theories of hypoelasticity, hyperelasticity, plasticity, fracture mechanics, plastic–fracture, or continuum damage, to name only some of the more popular ones. The present work will make use of a *continuum damage model* to characterize the mechanical behaviour of concrete. The Continuum Damage Theory was firstly intoduced by Kachanov (1958) in the context of creep–related problems, but it has afterwards been accepted as a valid alternative to deal with complex material behaviour. It is nowadays used for materials so different as metals, ceramics, rock and concrete, and within a wide range of applications (creep, fatigue, progressive failure, etc.). The reason for its popularity is as much the intrinsic simplicity and versatility of the approach, as well as its consistency, based on the theory of thermodynamics of irreversible processes.

Among the different possibilities that such a framework offers (Lemaitre and Chaboche 1978; Lemaitre 1984; Chaboche 1988a,b; Simó and Ju 1987a,b; Mazars and Pijaudier-Cabot 1989), this work will make use of an *isotropic damage model*, with only two scalar internal variables to monitor the local damage under tension and compression, respectively. This

will provide a simple constitutive model which, nevertheless, is able to capture the overall non–linear behaviour of concrete including strain–softening response and stiffness degradation and regradation under multiple stress reversals. Furthermore, the model can be implemented in a strain–driven form which leads to an almost closed–form algorithm to integrate the stress tensor in time. This is a most valuable feature for a model intended to be used in large scale computations. The damage model presented here is an extension of the one described in Cervera et al. (1995, 1996) and Faria et al. (1998), extended to account for temperature effects and the phenomenon of aging. For simplicity, only the rate independent format of the model will be considered, and no plastic deformations will be included.

Effective Stresses

The Continuum Damage Mechanics Theory (CDMT) is based on the definition of the effective stress concept, which is introduced in connection with the hypothesis of strain equivalence (Lemaitre and Chaboche 1978): the strain associated with a damaged state under the applied stress σ is equivalent to the strain associated with its undamaged state under the effective stress $\bar{\sigma}$. In the present work the (second order) effective stress tensor $\overline{\boldsymbol{\sigma}}$ will assume the following hyper-elastic form:

$$\overline{\boldsymbol{\sigma}}\,(\boldsymbol{\varepsilon}_e, \kappa) = \boldsymbol{D}(\kappa) : \boldsymbol{\varepsilon}_e \tag{1}$$

where $\boldsymbol{\varepsilon}_e$ is the (second order) elastic strain tensor, $\boldsymbol{D}(\kappa)$ is the usual (fourth order) linear–elastic constitutive tensor and (:) denotes the tensorial product contracted on two indices.

As our aim is to use a scalar damage model with separated internal damage variables for tensile and compressive stress contributions, a split of the *effective* stress tensor into tensile and compressive components is needed. In order to identify clearly contributions with respect to each one of these independent effective stress tensors, (+) and (–) indices will be extensively used, referring to tensile and compressive entities, respectively. In this work, the stress split will be performed as in Cervera et al. (1995, 1996) and Faria et al. (1998):

$$\begin{aligned} \overline{\boldsymbol{\sigma}}^{+} &= <\overline{\boldsymbol{\sigma}}> = \sum_{j=1}^{3} <\overline{\sigma}_j> \boldsymbol{p}_j \otimes \boldsymbol{p}_j \\ \overline{\boldsymbol{\sigma}}^{-} &= >\overline{\boldsymbol{\sigma}}< = \sum_{i=j}^{3} >\overline{\sigma}_j< \boldsymbol{p}_j \otimes \boldsymbol{p}_j \end{aligned} \tag{2}$$

where $\overline{\sigma}_j$ denotes the *j–th* principal stress value from tensor $\overline{\boldsymbol{\sigma}}$, $\boldsymbol{p}_j$ represents the unit vector associated with its respective principal direction and the symbol $\otimes$ denotes the tensorial product. The symbols $< \, . \, >$ are the Macaulay brackets ($< x >= x$, if $x \geq 0, < x >= 0$, if $x < 0$) and symbols $> \, . \, <$ are such that $> x <= x$, if $x < 0, > x <= 0$, if $x \geq 0$.

Free Energy and Constitutive Equation

In this Section we will consider the short term mechanical behaviour of concrete. The denomination "short term" is used in relation to the time

scale in which the hydration and aging phenomena take place, that is, the mechanical loading process will be considered as instantaneous (compared to the chemical and aging phenomena, see Part I). This means that, without loss of generality, the mechanical model can be defined assuming that the aging degree has a fixed value, $\kappa = \bar{\kappa}$. In consequence, all the related mechanical properties are also considered at fixed values: $f^-(\bar{\kappa})$, $f^+(\bar{\kappa})$, $E(\bar{\kappa})$, $G_f^+(\bar{\kappa})$ and $G_f^-(\bar{\kappa})$. Therefore, the free energy and the constitutive equation will not be considered explicitely dependent on the hydration and aging degrees, ξ and κ. Also, and consequently, all terms depending on their time derivatives, $\dot{\xi}$ and $\dot{\kappa}$, will be neglected in the definition of the mechanical dissipation. An extended model, applicable to the modelling of long term mechanical behaviour (under sustained loading) will be described in the next Section.

Let us define the elastic free energies associated with the tensile and compressive effective stresses in the form

$$W_e^{\pm} = W_e^{\pm}(\boldsymbol{\varepsilon}_e) = \frac{1}{2}\,\overline{\boldsymbol{\sigma}}^{\pm} : \boldsymbol{D}^{-1} : \overline{\boldsymbol{\sigma}} \tag{3}$$

where the superindex $(\pm)$ may mean tension or compression, as convenient. Some algebra is needed to show that $W_e^{\pm} \geq 0$. Let us also introduce two internal-like variables, d^+ and d^-, the damage indices under tension and compression, respectively, whose definition and evolution in terms of the real internal variables will be given later. Extending the concepts introduced in Faria et al. (1998), the mechanical free energy term for the damage model is defined by combining these elements in the form:

$$\begin{aligned} \Psi &= W(\boldsymbol{\varepsilon}_e, d^+, d^-) \\ &= W^+(\boldsymbol{\varepsilon}_e, d^+) + W^-(\boldsymbol{\varepsilon}_e, d^-) \\ &= (1-d^+)W_e^+(\boldsymbol{\varepsilon}_e) + (1-d^-)W_e^-(\boldsymbol{\varepsilon}_e) \end{aligned} \tag{4}$$

From this, and provided that $0 \leq d^+, d^- \leq 1$, it can be shown that $W \geq 0$ (Faria et al. 1998).

The constitutive equation for the damage model is obtained using Coleman's method as:

$$\boldsymbol{\sigma} = \partial_{\boldsymbol{\varepsilon}_e}\Psi = (1-d^+)\,\overline{\boldsymbol{\sigma}}^+ + (1-d^-)\,\overline{\boldsymbol{\sigma}}^- \tag{5}$$

The mechanical dissipation can be expressed as

$$\mathcal{D}_{mech} = W_e^+ \dot{d}^+ + W_e^- \dot{d}^- \geq 0 \tag{6}$$

provided that the damage indices increase monotonically, $\dot{d}^+, \dot{d}^- \geq 0$.

Characterization of Damage

In order to clearly define concepts such as loading, unloading, or reloading for general 3D stress states, a scalar positive quantity, termed as *normalized equivalent stress*, will be defined. This will permit the comparison of different 3D stress states, even for different degrees of hydration. With such a definition, distinct tridimensional stress states can be mapped to a single *normalized equivalent unidimensional stress test*, which makes their quantitative comparison possible.

As a consequence of the stress split, two separate equivalent effective stress norms are necessary: a normalized equivalent effective tensile norm τ^+, and a normalized equivalent effective compressive norm τ^-. In the present work they will assume the following form:

$$\tau^{\pm} = \left[\left(\frac{\overline{\boldsymbol{\sigma}}^{\pm}}{f_e^{\pm}} \right) : \boldsymbol{C}^{\pm} : \left(\frac{\overline{\boldsymbol{\sigma}}}{f_e^{\pm}} \right) \right]^{1/2} = \frac{1}{f_e^{\pm}} \left[\overline{\boldsymbol{\sigma}}^{\pm} : \boldsymbol{C}^{\pm} : \overline{\boldsymbol{\sigma}} \right]^{1/2} \tag{7}$$

where two non-dimensional fourth order metric tensors $\boldsymbol{C}^{\pm}$ have been introduced. Tensors $\boldsymbol{C}^{\pm}$ do not depend on the aging degree. The role of these tensors is to define the shape of the damage bounding surfaces in a normalized effective stress space, as it will be explained below. Note that the two metric tensors can be different for the tensile and compressive norms, $\boldsymbol{C}^+$ and $\boldsymbol{C}^-$, respectively.

The normalizing factors $f_e^{\pm}(\bar{\kappa})$ are introduced in Eq. (7) to account for the dependency of the mechanical strengths on the aging degree. From the physical point of view, they represent the values of the tensile f_e^+ and compressive f_e^- uniaxial stresses that define the onset of damage under uniaxial tension and compression, respectively. These values can be taken as proportional to the corresponding peak strengths $f^{\pm}$ defined by the aging model (see Part I) as $f_e^-(\bar{\kappa}) = \lambda_e^- f^-(\bar{\kappa})$ and $f_e^+(\bar{\kappa}) = \lambda_e^+ f^+(\bar{\kappa})$, respectively.

With the above definitions for the equivalent effective stresses, two separated damage criteria, g^+ and g^-, are introduced for tension and compression, respectively:

$$g^{\pm}\left(\tau^{\pm}, r^{\pm}\right) = \tau^{\pm} - r^{\pm} \leq 0 \tag{8}$$

Variables r^+ and r^- are normalized internal strain-like variables which can be interpreted as current damage thresholds, in the sense that their values control the size of the (monotonically) expanding damage surfaces. Due to its normalized nature, the initial values are unitary, $r_0^+ = r_0^- = 1$.

This means that the damage criteria are defined in a normalized effective stress space (or in a normalized strain space). The shape of the two damage bounding surfaces in the normalized effective stress space does not depend on the aging degree. This is a very attractive feature of the present normalized format for the damage model. In fact, the shape of the damage criteria is defined by the metric tensors $\boldsymbol{C}^{\pm}$. These tensors must be isotropic and positive definite, in the form:

$$\boldsymbol{C}^{\pm} = (1 + \gamma^{\pm})\, \boldsymbol{I} - \gamma^{\pm}\, \mathbf{1} \otimes \mathbf{1} \qquad \text{with} \qquad 0 \leq \gamma^{\pm} < 1 \tag{9}$$

where $\boldsymbol{I}$ is the fourth order unit tensor, $\mathbf{1}$ is the second order unit tensor and $\gamma^{\pm}$ is a parameter related to the equibiaxial tensile/compressive strengths. Calling $\rho^{\pm}$ to the ratio between the biaxial and uniaxial strengths, it is

$$\gamma^{\pm} = 1 - \frac{1}{2\,(\rho^{\pm})^2} \tag{10}$$

Figure 1 shows a 2D representation of the damage criteria for two possible selections of these tensors: (a) $\gamma^{\pm} = 0$, $\boldsymbol{C}^{\pm} = \boldsymbol{I}$ represents a rounded Rankine-type of criterion with $\rho^{\pm} = 1/\sqrt{2} = 0.707$, while (b) $\gamma^{\pm} = 0.622$ represents a much more realistic criterion for concrete with $\rho^{\pm} = 1.15$. A third possibility is to use (c) $\gamma^{\pm} = \nu$, $\boldsymbol{C}^{\pm} = \overline{\boldsymbol{D}}^{-1} = (\boldsymbol{D}/E)^{-1}$, which represents criteria related to the (normalized) tensile and compressive elastic

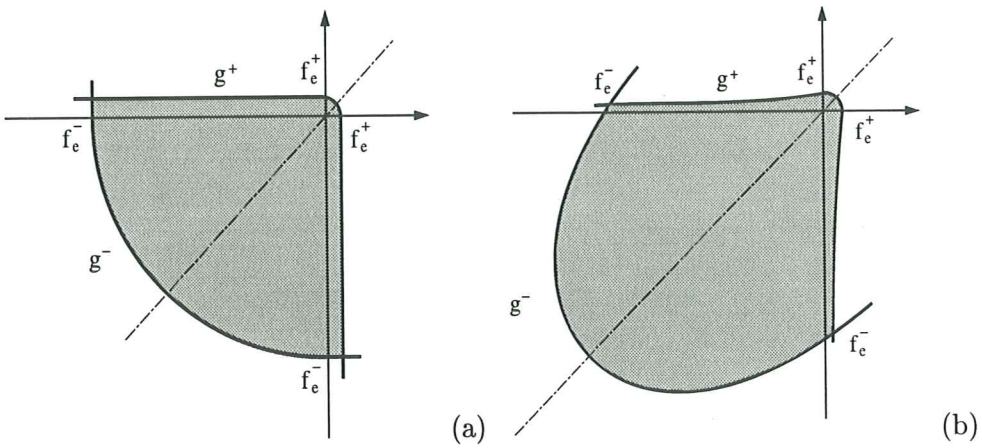

Figure 1: Two different damage criteria.

free energies, but leads to a quite small $\rho^{\pm} = 0.767$. Note that options (a) and (c) are identical if the effect of Poisson's ratio is disregarded.

The damage bounding surfaces defined in the normalized effective stress space by Eq. (8) can also be defined in the real effective stress space in the form

$$\hat{g}^{\pm}\left(\hat{\tau}^{\pm}, \hat{r}^{\pm}\right) = f_e^{\pm}\, g^{\pm}\left(\tau^{\pm}, r^{\pm}\right) = \hat{\tau}^{\pm} - \hat{r}^{\pm} \leq 0 \tag{11}$$

where $\hat{\tau}^{\pm}$ and $\hat{r}^{\pm}$ are unscaled versions of $\tau^{\pm}$ and $r^{\pm}$, respectively,

$$\hat{\tau}^{\pm} = \left[\,\overline{\boldsymbol{\sigma}}^{\pm} : \boldsymbol{C}^{\pm} : \overline{\boldsymbol{\sigma}}\,\right]^{1/2} \qquad \text{and} \qquad \hat{r}^{\pm} = f_e^{\pm}\, r^{\pm} \tag{12}$$

Therefore, it is clear that the scaling factors $f_e^{\pm}(\kappa)$ play the role of aging (chemical) hardening parameters, as they define the mapping of the damage bounding surfaces to the current effective stress space, and thus, the growth of their size as a result of the aging process. Since f_e^- and f_e^+ are not necessarily proportional (see Aging Model in Part I), the damage surfaces for different hardening degrees are not necessarily homothetical.

Figure 2 shows a 2D representation of the mapping of the damage criteria from (a) the normalized effective stress space to (b) the real effective stress space, in terms of the aging degree.

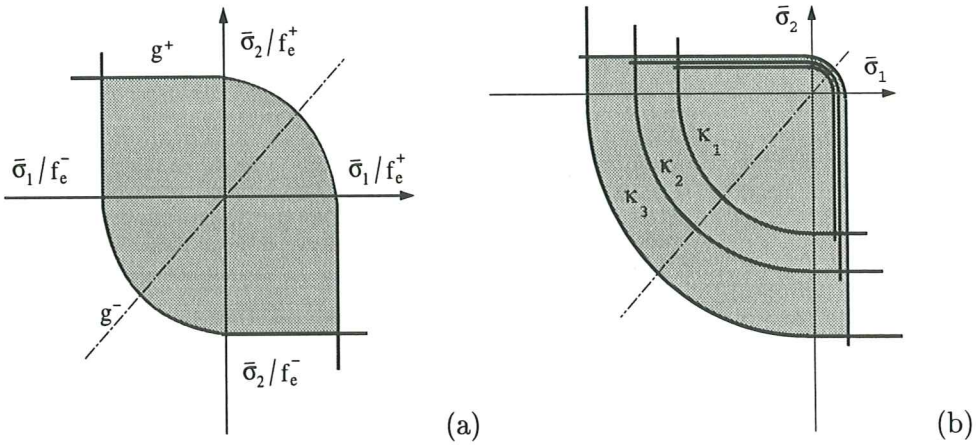

Figure 2: Mapping from the (a) normalized to the (b) real stress space.

Evolution of Damage

The evolution (expansion) of the damage bounding surfaces in the normalized space for loading, unloading and reloading conditions is controled by the Kuhn-Tucker relations and the damage consistency condition, which can be written as

$$\dot{r}^{\pm} \geq 0 \qquad g^{\pm} \leq 0 \qquad \begin{aligned} \dot{r}^{\pm}\, g^{\pm} &= 0 \\ \dot{r}^{\pm}\, \dot{g}^{\pm} &= 0 \end{aligned} \tag{13}$$

leading, in view of Eq. (8), to the loading condition $\dot{r}^{\pm} = \dot{\tau}^{\pm}$. This, in turn, leads to the explicit definition of the current values of the internal variables in the form

$$r^{\pm} = \max\left[r_0^{\pm}, \max(\tau^{\pm})\right] \tag{14}$$

Note that Eq. (14) allows to compute the current values for $r^{\pm}$ in terms of the current values of $\tau^{\pm}$, which in turn, depend explicitly on the current strains, temperature and degree of aging (see Eqs. (1) and (7)). For a given degree of aging, an increase of the elastic strains (and, consequently, effective stresses) would lead to an expansion of the bounding surfaces due to the evolution (increase) of damage. Alternatively, for a given state of strain and corresponding $r^{\pm}$ values, an increase in the aging degree would lead to an expansion of the bounding surfaces *without* evolution of damage (this is called chemical hardening).

Finally, the damage indices d^{+} and d^{-} are explicitly defined in terms of the corresponding current values of the damage thresholds, so that they are monotonically increasing functions such that $0 \leq d^{\pm}(r^{\pm}) \leq 1$. Let us drop the superindex $(\pm)$ in the following for the sake of brevity, and let us introduce the values $r_e = 1/\lambda_e = f(\bar{\kappa})/f_e(\bar{\kappa})$, establishing the size of the bounding damage surface for the onset of damage and $r_p \geq r_e$, establishing the size of the bounding damage surface at peak strength. These two values define the strain-hardening part of the uniaxial stress-strain curve for the material. Note that necessarily $r_p \geq r_e \geq r_0 = 1$. For the limit case $r_p = r_e = r_0 = 1$ the material would exhibit softening immediately after the onset of damage, which is an option often used for tension strain-softening.

In this work, we will use the functions

$$d(r) = A_d \frac{r_e}{r}\left(\frac{r-1}{r_p-1}\right)^2 \qquad r_0 \leq r \leq r_p \tag{15}$$

$$d(r) = 1 - \frac{r_e}{r}\exp\frac{1}{B_d}\left(\frac{r-r_p}{r_e}\right) \qquad r_p \leq r \tag{16}$$

where the constants A_d and B_d are defined as

$$A_d = \frac{r_p - r_e}{r_e} \tag{17}$$

$$B_d = \frac{1}{2}\frac{r_p}{r_e} - \frac{1}{l^*}\frac{EG_f}{f^2} + \overline{B}_d \tag{18}$$

where $\overline{B}_d = A_d\,(r_p^3 - 3r_p + 2)\,/\,6\,r_e\,(r_p-1)^2$. In Eq. (18) the fracture energies (under tension and compression) of the material G_f and the characteristic

length l^* have been introduced to ensure mesh-size objective results (Oliver 1989).

Note that the dependence of the fracture energies on the aging degree defined by the aging model (see Part I) imply that the fraction EG_f/f^2 is be independent of κ, so that $EG_f/f^2 = E_\infty G_{f\infty}/f_\infty^2$, where the subscript (∞) means values at the end of the hydration process. This means that the parametre B_d is independent of the aging degree.

Note also, that for the limit case $r_0 = r_e = r_p$, Eqs. (17) and (18) yield $A_d = 0$ and $B_d = 1/2 - EG_f/l^* f^2$, a well-known result for exponential softening (Cervera et al. 1995, 1996).

Figure 3(a) shows a schematic representation of a uniaxial stress vs. strain curve, which explains the role of parameters r_e and r_p. Figure 3(b) shows the evolution of the stress vs strain curves for different increasing aging degrees.

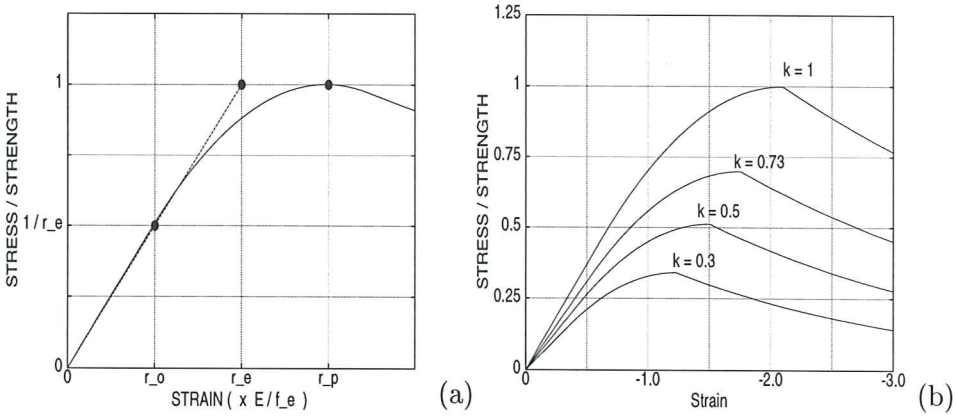

Figure 3: Uniaxial stress-strain curves.

Thermal and Chemical Coupling

In order to account for thermo-mechanical and chemo-mechanical effects, the (second order) elastic strain tensor $\boldsymbol{\varepsilon}_e$ is redefined as:

$$\boldsymbol{\varepsilon}_e(\boldsymbol{\varepsilon}, T, \xi) = \boldsymbol{\varepsilon} - [\alpha_T (T - T_{ref}) + \alpha_\xi \xi] \mathbf{1} \tag{19}$$

where $\boldsymbol{\varepsilon}$ is the (second order) total strain tensor, α_T and α_ξ are the thermal and chemical volumetric change coefficients, respectively, and $\mathbf{1}$ is a (second order) unit tensor. The reference temperature T_{ref} can be taken as equal to the temperature reached at the end of the setting phase (when $\xi = \xi_{set}$), so that the thermal stressing initiates then.

With this redefinition, the above given expressions for the effective stresses, Eq. (1), the mechanical part of the free energy, Eq. (4), the constitutive equation, (Eq. (5), and the mechanical dissipation, Eq. (6), remain identical.

LONG TERM MECHANICAL BEHAVIOUR

The mechanical model introduced in the previous Section is able to describe the short term mechanical behaviour of concrete at early ages. In

this Section the inclusion of the long term behaviour, or behaviour under sustained loading, will be addressed. The basic idea is to use a viscoelastic aging model, able to reproduce the creep and relaxation phenomena typical of long term behaviour of concrete. This must be coupled to the damage model described above, also considering the relevant thermal and chemical effects.

As in the long term behaviour the time scale in which the loading takes place is comparable to that in which the hydration and aging processes occur, both the hydration and aging degrees will be explicitely considered in the definition of the model.

Solidification Theory

In classical viscoelasticity, the mechanical behaviour is characterized by the relaxation function or the compliance function and the constitutive relationships are formulated in the form of Volterra integral equations (Bazant 1988). This approach is clearly unsuitable for numerical computations because of its memory and CPU time requirements.

Following previous work regarding the long term behaviour of concrete (Cervera et al. 1992), and the recommendations of Carol and Bazant (1993), we will consider the relaxation function of concrete expanded into a Dirichlet series, and retain only a finite number of terms, say N. This achieves a double goal: first, the constitutive laws for the viscoelastic material can be written in terms of a finite number of internal variables, and only these need to be stored from one time step to the next, thus providing huge computational advantages compared to the hereditary integral equations; and secondly, the resulting rheological model can be interpreted as a generalized Maxwell chain, where a number of springs and dashpots are arranged in parallel. Alternatively, the compliance function of concrete can be considered and expanded in a Dirichlet series. This leads to a generalized Kelvin chain with a series arrangement (see Bazant and Prasannan 1989; Carol and Bazant 1993; Bazant et al. 1997).

Although both approaches are completely equivalent (if a large enough number of terms is considered in the Dirichlet series), the first one leads to first order differential equations to be solved for the evolution of the internal variables, while the second approach leads to second order differential equations. Therefore, the Maxwell chain model is preferred here, with the elastic moduli, E^i, and the dashpot viscosities, η^i, of the $i = 1, ..., N$ Maxwell elements of the chain as material parameters. It is also helpful to consider the elastic moduli, E^i, and the relaxation times of the dashpots, defined as $\tau^i = \eta^i / E^i$, as an alternative characterization of the chain. It is convenient to take $\tau^1 = \infty$ in the series expansion, so that E^1 can be considered as the *asymptotic* elastic modulus of concrete.

Figure 4 shows a schematic representation of the rheological model used for long term behaviour, in the form of a Maxwell chain. In the framework of aging models the general case of such a rheological model would consist of independently varying elastic moduli and dashpot viscosities. However, it is usual to restrict the model to the consideration of proportional varying elastic moduli and constant relaxation times. This greatly reduces the complexity and mathematical difficulties of determining the material pa-

rameters, as well as preventing the controversial topic of the divergence of the creep curves for different ages at loading (Carol and Bazant 1993).

In the following we will assume that during the aging process all the elastic moduli vary proportionally to the aging function defined by the aging model, $E^i(\kappa) = \lambda_E(\kappa)\, E^i_\infty$ (where E^i_∞ are values at the end of the hydration process, and $E_\infty = \sum_{i=1}^N E^i_\infty$), and that the relaxation times, τ^i, remain constant. It was shown in Carol and Bazant (1993) that this is equivalent to the model arising from Solidification Theory (Bazant and Prasannan 1989) with a non-aging Maxwell chain for the basic constituent. The total stress sustained by the Maxwell chain is easily computed as

$$\boldsymbol{\sigma} = \sum_{i=1}^{N} \boldsymbol{\sigma}^i \tag{20}$$

Choosing the stress in each Maxwell element of the chain, $\boldsymbol{\sigma}^i$, as internal variables, it was shown there that the first order differential equations governing the evolution of these variables are

$$\dot{\boldsymbol{\sigma}}^i + \frac{\boldsymbol{\sigma}^i}{\tau^i} = \lambda_E(\kappa) E^i_\infty \overline{\boldsymbol{D}}\, \dot{\boldsymbol{\varepsilon}} \quad \text{for} \quad i = 1, ..., N \tag{21}$$

where tensor entities are used as the multidimensional counterparts of the scalar ones used for uniaxial models; $\boldsymbol{\varepsilon}$ is the total strain tensor and the non-dimensional tensor $\overline{\boldsymbol{D}} = (1/E)\boldsymbol{D}$ has been used.

The basic assumption in the derivation of Eq. (21) and behind Solidification Theory is that when new layers of material solidify, they join the previously existing in a parallel coupling. We have identified the nondimensional solidified fraction function $v(t)$ introduced in Bazant (1977) with the elastic modulus aging function $\lambda_E(\kappa)$ introduced in the aging model.

Micro-prestress Theory

The proposed model (and the underlying Solidification Theory) cannot be the final solution of the long term aging because the duration of creep for

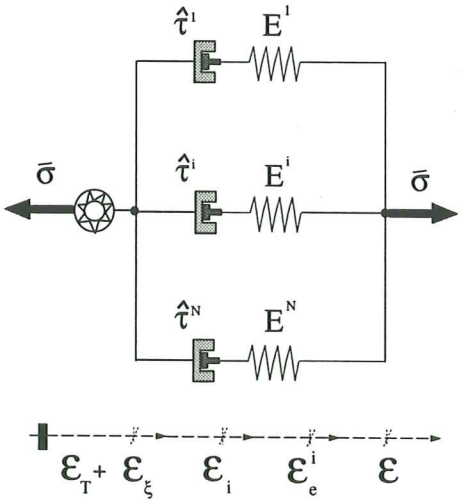

Figure 4: Rheological model for long term behaviour.

a fixed load decreases significantly with an increasing age at loading even after many years, while the hydration degree essentially stops before one year of age. This experimental evidence was considered in the Solidification Theory (Bazant and Prasannan 1989) by including a *flow element* with a time dependent viscosity connected in series to an aging Kelvin chain. In Bazant et al. (1997b) a more fundamental approach is followed to justify the physical existence of such flow term. A physical model is formulated to obtain the viscosity of the flow dashpot as a function of the tensile micro-prestress carried by the bonds and bridges crossing the gel pores in the hardened cement gel. The long term creep is assumed to originate from viscous shear slips between the opposite walls of micropores in which the bonds that transmit the micro-prestress break and reform. Let σ_μ be the value of the micro-prestress and η_μ be the value of the viscosity of the corresponding flow term.

Let $\sigma_{\mu 0}$ and $\eta_{\mu 0}$ be their initial values. Let us assume that the viscosity is inversally proportional to the micro-prestress, so that

$$\frac{\sigma_\mu}{\sigma_{\mu 0}} = \frac{\eta_{\mu 0}}{\eta_\mu} = \mu \tag{22}$$

where μ is a variable that can be regarded as the normalized value of the micro-prestress. Note that initially $\mu(t=0) = 1$. A nonlinear differential equation defining the evolution of μ in terms of the relative humidity, h, and its variation, $\dot{h}$, may be written as (Bazant et al. 1997b)

$$\dot{\mu} + c_{\mu 0}\,\mu^2 = -\,c_{\mu 1}\,\frac{\dot{h}}{h} \tag{23}$$

where $c_{\mu 0}$ and $c_{\mu 1}$ are material properties. If humidity effects are not considered (sealed specimens, basic creep), Eq. (23) reduces to

$$\dot{\mu} = -\,c_{\mu 0}\,\mu^2 \tag{24}$$

which can be integrated in time to obtain the evolution of the normalized micro-prestress:

$$\mu(t) = \frac{1}{1 + c_{\mu 0}\,t} \tag{25}$$

Then the viscosity can be computed as $\eta_\mu = \eta_{\mu 0}/\mu$. Note that as time increases, the micro-prestress decreases, and so the viscosity of the flow term increases. Eventually, the micro-prestress will vanish, the viscosity will reach tend to infinity and the flow term will become inactive.

Although in the mentioned references the flow element was connected in series to a Kelvin chain with aging elastic moduli, the same behaviour can be obtained with a generalized Maxwell chain with aging elastic moduli. To this end let us *define* the relaxation time of the flow term as

$$\tau_\mu = \frac{\eta_\mu}{E} = \frac{\eta_{\mu 0}/\mu}{\lambda_E\,E_\infty} = \frac{\tau_{\mu 0}}{\lambda_E\,\mu} \tag{26}$$

where $\tau_{\mu 0} = \eta_{\mu 0}/E_\infty$ is a material property. Now, Eq. (21) has to be modified to include the effect of the nonlinear flow term:

$$\dot{\boldsymbol{\sigma}}^i + \left(\frac{1}{\tau^i} + \frac{1}{\tau_\mu}\right)\boldsymbol{\sigma}^i = E^i(\kappa)\,\overline{\boldsymbol{D}}\,\dot{\boldsymbol{\varepsilon}} \quad \text{for} \quad i = 1, ..., N \tag{27}$$

Note that the effect of the flow term is completely defined with two additional material properties: $\tau_{\mu 0}$ and $c_{\mu 0}$. The first one defines the initial value of the viscosity, and the second one governs its rate of evolution.

Viscous strains

In the following, we will select the viscous strains in each Maxwell element, $\boldsymbol{\varepsilon^i}$, rather than the stress, $\boldsymbol{\sigma^i}$, as internal variables. The relationship between them is

$$\boldsymbol{\sigma}^i = E^i(\kappa)\,\overline{\boldsymbol{D}} : (\boldsymbol{\varepsilon} - \boldsymbol{\varepsilon}^i) \tag{28}$$

Substitution of Eq. (28) into Eq. (27) leads to the obtention of the evolution law for the viscous strains

$$\dot{\boldsymbol{\varepsilon}}^i = \Big(\frac{1}{\tau^i} + \frac{1}{\tau_\mu} + \frac{1}{\tau_a}\Big)(\boldsymbol{\varepsilon} - \boldsymbol{\varepsilon}^i) = \frac{1}{\hat{\tau}^i}(\boldsymbol{\varepsilon} - \boldsymbol{\varepsilon}^i) \qquad \text{for} \quad i = 1, ..., N \tag{29}$$

with $\tau_a(\kappa) = \lambda_E/\dot{\lambda}_E$ representing the aging effect on the elastic modulus. Note that even if τ^i and τ_μ are sufficiently large, there would be some viscous straining as long as the aging progresses and the elastic modulus varies ($\dot{\lambda}_E \neq 0$). As time increases, the rate of hydration decreases, and so the viscosity due to aging increases. Eventually, $\tau_a(t = \infty) = \infty$ and the model would revert to a standard Maxwell viscoelastic arrangement.

Eq. (29) represents the evolution law for the viscous strains. Details on the numerical integration of Eq. (29) are given in Cervera and al. (1992) and Galindo (1993).

Thermodynamic Framework

In the long term behaviour of concrete both the hydration and aging degrees, ξ and κ, play a significant role, and consequently, they will be explicitely considered in the definition of the free energy of the model and in the state equations. Also, the corresponding terms depending on their time derivatives will be considered in the expression of the mechanical dissipation.

Let us define the elastic free energy associated to each element in the Maxwell chain in the form

$$\begin{aligned} W_e^i &= W_e^i(\boldsymbol{\varepsilon}_e^i, \kappa) \\ &= \frac{1}{2}\,\boldsymbol{\sigma}^i : (E^i(\kappa)\,\overline{\boldsymbol{D}})^{-1} : \boldsymbol{\sigma}^i \\ &= \frac{1}{2}\,\boldsymbol{\varepsilon}_e^i : (E^i(\kappa)\,\overline{\boldsymbol{D}}) : \boldsymbol{\varepsilon}_e^i \end{aligned} \tag{30}$$

where the elastic strain tensor is defined as $\boldsymbol{\varepsilon}_e^i = \boldsymbol{\varepsilon} - \boldsymbol{\varepsilon}^i$, for each Maxwell element.

The total free energy associated to the Maxwell chain is obtained by adding the contributions of the elements

$$W_e = W_e(\boldsymbol{\varepsilon}_e^i, \kappa) = \sum_{i=1}^{N} W_e^i(\boldsymbol{\varepsilon}_e^i, \kappa) \tag{31}$$

Using Coleman's method, the total stress can be obtained from this expression as

$$\boldsymbol{\sigma} = \partial_{\boldsymbol{\varepsilon}_e} W_e = \sum_{i=1}^{N} \partial_{\boldsymbol{\varepsilon}_e} W_e^i = \sum_{i=1}^{N} E^i(\kappa)\,\overline{\boldsymbol{D}} : \boldsymbol{\varepsilon}_e^i = \sum_{i=1}^{N} \boldsymbol{\sigma}^i \tag{32}$$

Note that the introduced viscous strains $\boldsymbol{\varepsilon}^i$ are the thermodynamical forces conjugated to the stresses in the chain elements $\boldsymbol{\sigma}^i$ ($\boldsymbol{\sigma}^i = -\partial_{\boldsymbol{\varepsilon}^i} W_e$).

Also, the mechanical dissipation for the Maxwell chain can be computed as

$$\mathcal{D}_{mech} = \sum_{i=1}^{N} \left(\frac{2}{\tau^i} + \frac{2}{\tau_\mu} + \frac{1}{\tau_a} \right) W_e^i \geq 0 \tag{33}$$

where τ^i, τ_μ, τ_a and W_e^i have already been defined.

Aging Viscoelasticity and Damage

Finally, let us consider the coupling of the viscoelastic model described above with the aging damage model described in Section , as well as including the relevant thermal and chemical couplings.

The basic hypothesis is that the stress sustained by the Maxwell chain is the effective (undamaged) stress, rather than the total stress. This idea is based on the CDMT concept that it is the effective stress the one acting on the effective (undamaged) solid concrete, while the total stress acts on the whole (damaged) solid.

Let us begin by defining the effective stresses and the elastic strains for one element of the Maxwell chain analogously to Eqs. (1) and (19):

$$\overline{\boldsymbol{\sigma}}^i \left(\boldsymbol{\varepsilon}_e^i, \kappa \right) = E^i(\kappa)\, \overline{\boldsymbol{D}} : \boldsymbol{\varepsilon}_e^i \tag{34}$$

with

$$\boldsymbol{\varepsilon}_e^i(\boldsymbol{\varepsilon}, \boldsymbol{\varepsilon}^i, T, \xi) = \boldsymbol{\varepsilon} - \boldsymbol{\varepsilon}_T - \boldsymbol{\varepsilon}_\xi - \boldsymbol{\varepsilon}^i \tag{35}$$

where the thermal, $\boldsymbol{\varepsilon}_T = \alpha_T (T - T_{ref})\, \mathbf{1}$, and chemical, $\boldsymbol{\varepsilon}_\xi = \alpha_\xi \xi\, \mathbf{1}$, volumetric strains affect all the elements in the same way, but the (second order) viscous strain tensor, $\boldsymbol{\varepsilon}^i$, is different for each Maxwell element. This means that the elastic strains and the effective stresses in the different chain elements will be neither proportional, nor co-rotational. Let us also define the stress split for each element, as

$$\overline{\boldsymbol{\sigma}}^{i+} = \sum_{j=1}^{3} < \overline{\sigma}_j^i > \boldsymbol{p}_j^i \otimes \boldsymbol{p}_j^i \qquad \text{and} \qquad \overline{\boldsymbol{\sigma}}^{i-} = \overline{\boldsymbol{\sigma}}^i - \overline{\boldsymbol{\sigma}}^{i+} \tag{36}$$

where $\overline{\sigma}_j^i$ denotes the *j–th* principal stress value from tensor $\overline{\boldsymbol{\sigma}}^i$, $\boldsymbol{p}_j^i$ represents the unit vector associated with its respective principal direction and the symbol $\otimes$ denotes the tensorial product. The symbols $< . >$ are the Macaulay brackets.

Let us define the elastic free energy associated with the tensile and compressive effective stresses for each element in the form

$$\begin{aligned} W_e^{i+} &= W_e^{i+}(\boldsymbol{\varepsilon}_e^i, \kappa) = \frac{1}{2}\, \overline{\boldsymbol{\sigma}}^{i+} : (E^i(\kappa)\, \overline{\boldsymbol{D}})^{-1} : \overline{\boldsymbol{\sigma}}^i \\ W_e^{i-} &= W_e^{i-}(\boldsymbol{\varepsilon}_e^i, \kappa) = \frac{1}{2}\, \overline{\boldsymbol{\sigma}}^{i-} : (E^i(\kappa)\, \overline{\boldsymbol{D}})^{-1} : \overline{\boldsymbol{\sigma}}^i \end{aligned} \tag{37}$$

Some algebra is needed to show that $W_e^{i+}, W_e^{i-} \geq 0$ (see Faria et al. 1998 for details). The total elastic free energy associated to the Maxwell

chain is obtained by adding the contributions of the elements

$$\begin{aligned} W_e &= W_e(\varepsilon_e^i, \kappa) \\ &= W_e^+(\varepsilon_e^i, \kappa) + W_e^-(\varepsilon_e^i, \kappa) \\ &= \sum_{i=1}^{N} W_e^{i+}(\varepsilon_e^i, \kappa) + \sum_{i=1}^{N} W_e^{i-}(\varepsilon_e^i, \kappa) \end{aligned} \tag{38}$$

Introducing the damage indices under tension and compression d^+ and d^-, respectively, the mechanical free energy term is defined by combining previously defined items in the form:

$$\begin{aligned} W &= W(\varepsilon_e^i, \kappa, d^+, d^-) \\ &= W^+(\varepsilon_e^i, \kappa, d^+, d^-) + W^-(\varepsilon_e^i, \kappa, d^+, d^-) \\ &= (1-d^+)\, W_e^+(\varepsilon_e^i, \kappa) + (1-d^-)\, W_e^-(\varepsilon_e^i, \kappa) \end{aligned} \tag{39}$$

Note that this term is very similar to that in Eq. (4), and it already includes the thermo-mechanical and chemo-mechanical couplings through Eqs. (34) and (35). It can be shown that $W \geq 0$.

The free energy for the complete thermo-chemo-mechanical model can be expressed in terms of two external variables, the strain tensor $\boldsymbol{\varepsilon}$ and the temperature T, the N viscous strain tensors $\boldsymbol{\varepsilon}^i$, the two damage indices, d^+ and d^-, and the hydration and aging degrees ξ and κ, in the form:

$$\begin{aligned} \Psi &= \Psi(\varepsilon_e^i, \kappa, d^+, d^-) \\ &= W(\varepsilon_e^i, \kappa, d^+, d^-) + V(T) + L(T, \xi) + H(\xi) \end{aligned} \tag{40}$$

where the thermal $V(T)$, the chemical $H(\xi)$ and the coupling thermo-chemical $L(T, \xi)$ terms were described in the hydration model.

The state equations for the thermo-chemo-mechanical model are obtained from Eq. (40) using Coleman's method. The expression for the entropy and the chemical affinity are:

$$S = -\partial_T \Psi = \frac{1}{T_0}\left[C(T - T_0) - Q(\xi)\right] \tag{41}$$

$$A_\xi = -\partial_\xi \Psi = k_\xi \left(\frac{A_{\xi 0}}{k_\xi \xi_\infty} + \xi\right)(\xi_\infty - \xi) \tag{42}$$

where the coupling terms $-\partial_T W$ in Eq. (41) and $-\partial_\xi L$, $-\partial_\xi W$ in Eq. (42) have been neglected because they can only be significant for very specific applications, with concrete subjected to high temperature and/or pressure.

The stresses are obtained as:

$$\begin{aligned} \boldsymbol{\sigma} = \partial_{\boldsymbol{\varepsilon}_e} \Psi &= \partial_{\boldsymbol{\varepsilon}_e} W^+ + \partial_{\boldsymbol{\varepsilon}_e} W^- \\ &= (1-d^+) \sum_{i=1}^{N} \overline{\boldsymbol{\sigma}}^{i+} + (1-d^-) \sum_{i=1}^{N} \overline{\boldsymbol{\sigma}}^{i-} \\ &= (1-d^+)\, \overline{\boldsymbol{\sigma}}^+ + (1-d^-)\, \overline{\boldsymbol{\sigma}}^- \end{aligned} \tag{43}$$

so that the same final form as in Eq. (5) is obtained for the damage model.

The definition of the damage surfaces and the evolution of the damage indices and thresholds can be done in terms of the total tensile and compressive parts of the effective stress, $\overline{\boldsymbol{\sigma}}^+$ and $\overline{\boldsymbol{\sigma}}^-$, as explained in the previous Section.

The total dissipation can be splitted into its chemical and mechanical parts, $\mathcal{D} = \mathcal{D}_{chem} + \mathcal{D}_{mech}$, with

$$\mathcal{D}_{chem} = A_\xi \dot{\xi} \geq 0 \tag{44}$$

$$\mathcal{D}_{mech} = \sum_{i=1}^{N} \left(\frac{2}{\tau^i} + \frac{2}{\tau_\mu} + \frac{1}{\tau_a} \right) W^i + W_e^+ \dot{d}^+ + W_e^- \dot{d}^- \geq 0 \tag{45}$$

provided that the elastic modulus and the damage indices increase monotonically, $\dot{\tau}_a, \dot{d}^+, \dot{d}^- \geq 0$.

NUMERICAL SIMULATIONS

This Section presents an assessment of the thermo-chemo-mechanical model described above. All the problems presented are solved advancing step-by-step in time. Solution of the purely chemo-mechanical problems consists of, for each time step, solving the mechanical equilibrium equation, together with the differential equation governing the chemical process (see Part I). Solution of the coupled thermo-chemo-mechanical problems consists of, for each time step, solving firstly the thermal equation, together with the differential equation governing the chemical process; and secondly, solving the mechanical problem, using the computed temperature and hydration degree fields (Prato et al. 1997).

Short term mechanical model

This Subsection is devoted to compare available experimental data with numerical predictions obtained using the thermo-chemo-mechanical model proposed above. The objective is to demonstrate that the model can adequately reproduce the evolution of the mechanical properties of concrete at early ages and predict the experimental stress versus strain reponse at different stages of the hydration process. Both isothermal and adiabatic conditions are considered.

The experimental tests were carried out at McGill University, Montreal, Canada (Khan et al. 1995). The samples were concrete cylinders, 100 x 200 mm., cast in special plastic cylinder molds designed to enable demolding at very early ages without disturbing the concrete. Details on the composition and properties of the concrete used are listed in Khan et al. (1995). Different concrete mixes were used in the experimental program in order to test low, medium and high strength concretes. We will consider two mixes: an ordinary Portland concrete, here referred to as C-30, and a high-strenth concrete, here referred to as C-100 (i.e. the approximate 28-days concrete strengths in MPa.). C-30 is a Type 10 cement concrete mix, without superplasticizer addition. C-100 used a Type 10 blended cement containing 9 % of silica fume and a high dosage of superplasticizer. Table 1 presents the numerical values that have been used for the numerical simulation of the tests. Note that the same material properties have been used to simulate the hydration process under adiabatic and isothermal curing conditions. This is intended to show the capability of the model to simulate properly the influence of temperature in the hydration and aging phenomena.

Properties	C-30	C-100
w/c	0.50	0.25
s/c	0.00	0.09
$C\ [J/m^3\,^oC]$	2.07 x 10^6	2.43 x 10^6
$k_T\ [J/m\,hs\,^oC]$	5207	6420
$T_0\ [^oC]$	21	21
ξ_∞	0.75	0.58
$k_\xi/\eta_{\xi 0}\ [1/hs]$	1.4 x 10^5	4.0 x 10^6
$\overline{\eta}$	7.5	6.0
$A_{\xi 0}/k_\xi$	1.0 x 10^{-4}	1.0 x 10^{-10}
$E_a/R\,[^oK]$	4000	4000
$Q_\xi\ [J/m^3]$	1.58 x 10^8	2.72 x 10^8
ξ_{set}	0.2	0.2
A_f	1.82	4.24
B_f	0.40	0.49
$f_\infty^-\,[MPa]$	34.5	109
$T_T\,[^oC]$	100	100
$T_{ref}\,[^oC]$	21	21
n_T	0.42	0.0
$E_\infty\,[GPa]$	29.6	46.4
r_e^-	2.76	2.72
r_p^-	4.74	3.74

Table 1: Material Properties for Short Term Mechanical Simulations.

Adiabatic Tests

For these tests a computer controlled temperature-matched curing technique was developed so that adiabatic conditions could be simulated. Details on the experimental set up can be obtained from Khan et al. (1995, 1998).

Figures 5 and 6 show results for the tests conducted on the C-30 and C-100 mixes, respectively. Figure 5(a) shows the comparison between the evolution of the temperature rise obtained from the model and that obtained in the experiment for the first 36 hours. The dots represent the experimental values, the solid line is the prediction by the model. Unfortunately, experimental temperatures beyond the first 24 hours can not be considered realistic, as a certain drop is reported. This is not possible in an adiabatic test, especially as a maintained increase in the compressive strength is measured until the seventh day of age. The fact can be related to heat losses due to conduction or other experimental fault. Even though, the agreement between the numerical and experimental results is good.

Figure 5(b) shows the evolution of the compressive strength with the hydration degree (adiabatic test). The solid line represents the results obtained from the simulation, while the black dots represent experimental values. The experimental values of the hydration degree are obtained from the experimental temperature rise versus time curve in the form indicated in Part I of the paper. A remarkable agreement is obtained over the whole time span of the experiment.

Figure 5(c) shows stress-strain curves for uniaxial compression tests carried out at different ages of the concrete. Only those curves obtained for

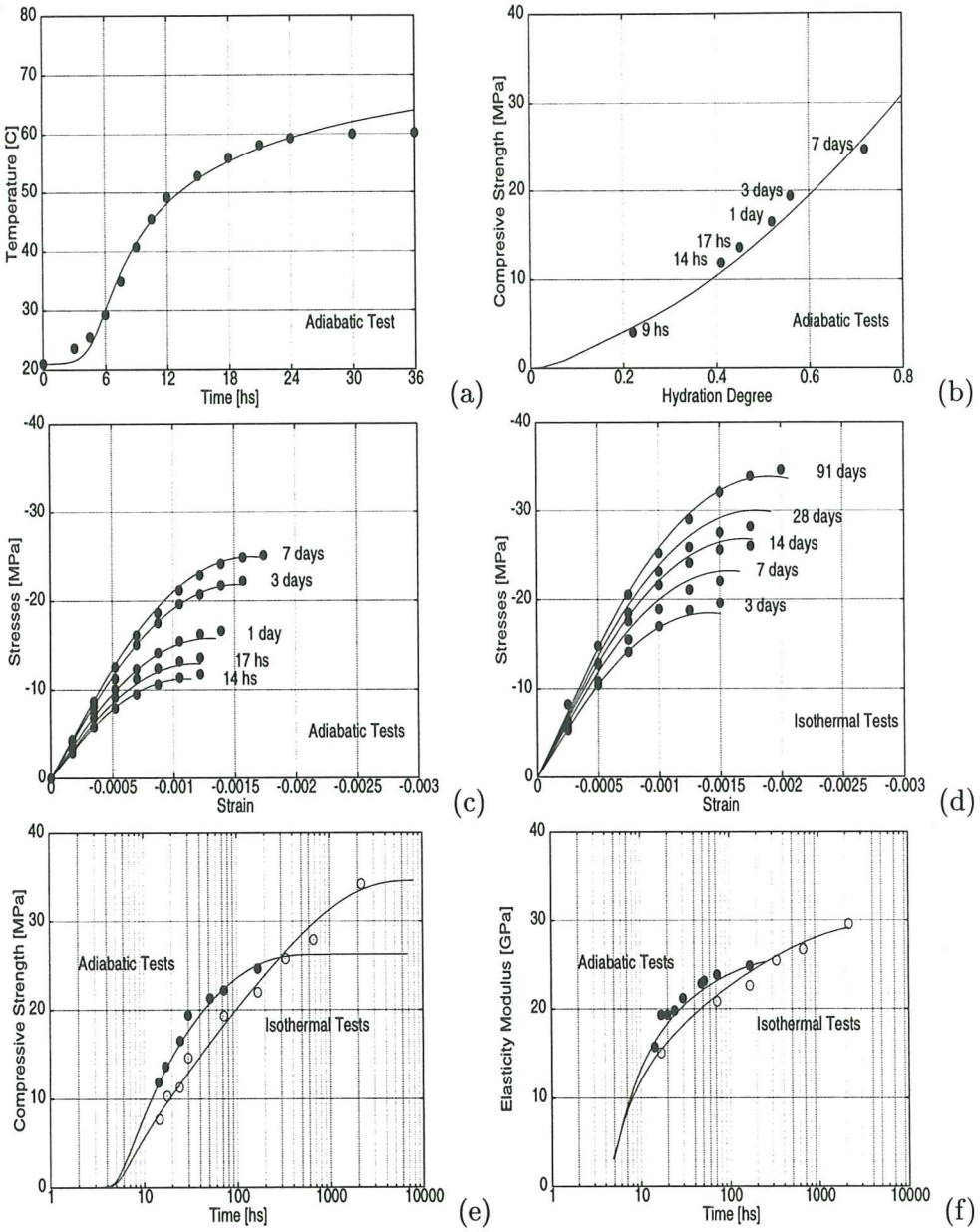

Figure 5: Results for C-30 concrete.

hydration degrees $\xi \geq 0.4$ have been selected for comparison. For lower values of the hydration degree the free water content in the mix is still high, and the experimental stress-strain curves exhibit a marked viscous character. The agreement between the computed and experimental results is remarkable, both in the prediction of the aging effect (corresponding to the evolution of the compressive strength and the elastic modulus) and in the description of the nonlinear part of the stress-strain curves. This shows how the proposed damage model agrees with the experimental behaviour. Only results up to peak strength are shown, as the behaviour during the strain-softening part of the curve would be dependent on the localization pattern in the samples, which is not reported from the experiments.

Figures 6(a), (b) and (c) show analogous results for the adiabatic tests performed with the C-100 concrete mix. As before, only those curves ob-

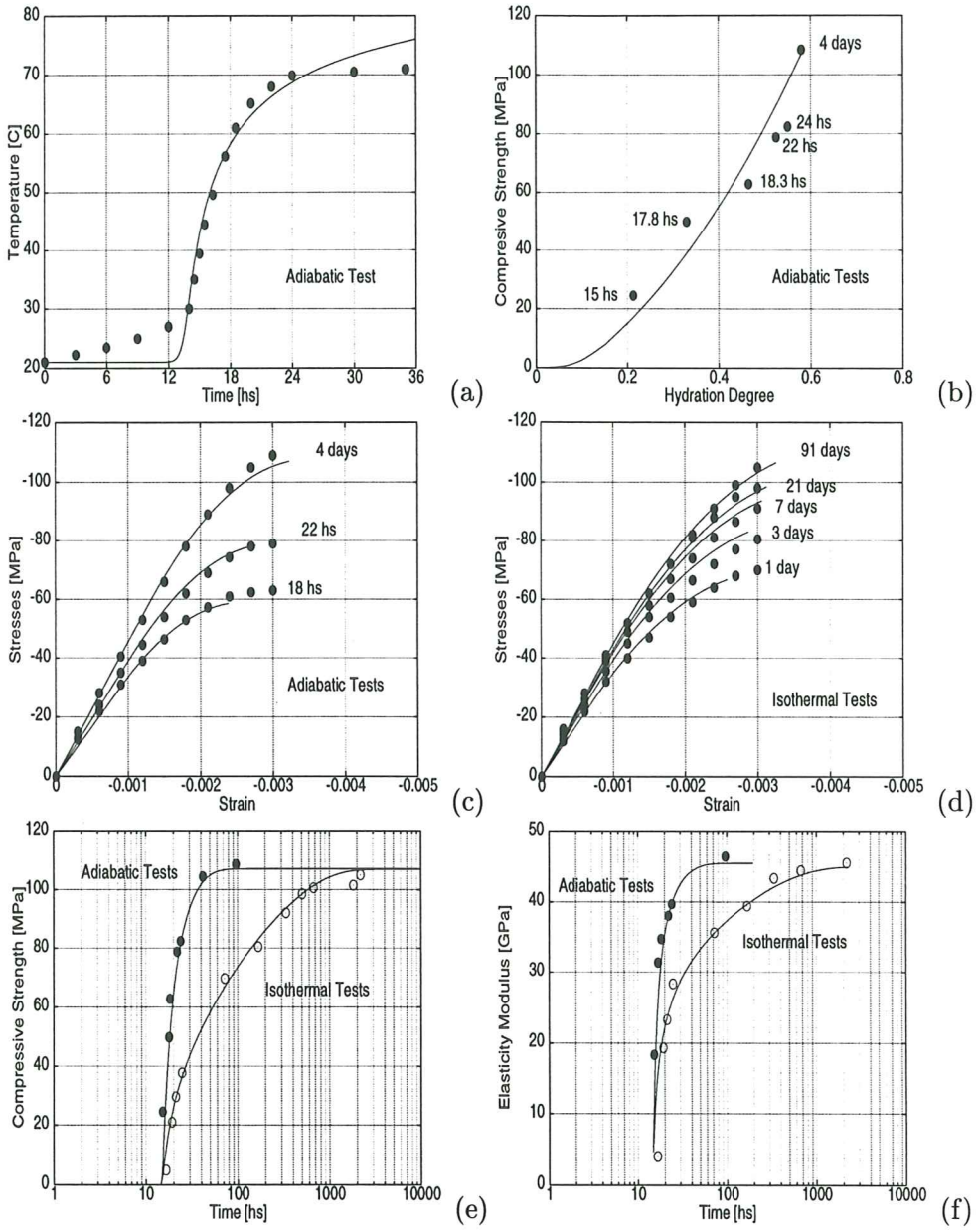

Figure 6: Results for C-100 concrete.

tained for hydration degrees $\xi \geq 0.4$ have been selected for comparison. Good overall agreement is achieved. Note how the model is able to reproduce the displayed retardation of hydration (more than 12 hours) due to the high dosage of superplasticizers used for this mix.

Isothermal Tests

The samples used in the isothermal tests were cured under sealed conditions achieved by wrapping the cylinders with polyfilm. The curing conditions are such that the temperature rise due to the hydration heat is not significant. This implies that the tests are carried out in (quasi) isothermal conditions.

Again, figures 5 and 6 show results for the tests conducted on the C-30 and C-100 mixes, respectively. Figure 5(d) shows stress-strain curves for uniaxial compression tests carried out at different ages of the concrete. The

agreement between the computed and experimental results is remarkable, both in the prediction of the aging effect (corresponding to the evolution of the compressive strength and the elastic modulus) and in the description of the nonlinear part of the curve. Figure 6(d) show analogous results for the isothermal tests performed with the C-100 concrete mix.

Figure 5(e) shows the evolution of the compressive strength with time, both for the adiabatic and isothermal tests. Note that even the same material properties have been used for the simulation of the hydration and aging phenomena, quite different results are obtained, depending on the curing conditions. Concrete gains strength more rapidly when subjected to adiabatic curing. On the other hand, the ultimate compressive strength attained under isothermal curing is 31 % higher than under adiabatic curing. Figure 5(f) shows the evolution of the elastic modulus with time, both for the adiabatic and isothermal tests. The observed evolution trend is very similar to the evolution of the compressive strength. Note that both the evolution of the compressive strength and the elastic modulus is very well captured by the proposed aging model. Figures 6(e) and (f) show analogous results for the adiabatic and isothermal tests performed with the C-100 concrete mix. Note that the effect of the curing temperature on the ultimate compressive strength is much smaller for high-performance concretes than for conventional concretes.

Results presented in this Subsection show the ability of the proposed model to capture the overall short term thermo-chemo-mech an ic al behaviour of concrete at early ages.

Long term mechanical model

This Subsection is devoted to compare available experimental data with numerical predictions obtained using the long term chemo-mechanical model proposed above. The objective is to demostrate that the model can adequately reproduce the evolution of the mechanical properties of concrete at early ages and predict the experimental strain versus time reponse for sustained loading applied at different stages of the aging process. Drying effects have not been considered in this work; thus, only basic creep experiments will be considered here for comparison. The experimental set ups for these experiments try to enforce isothermal conditions to exclude the influence of temperature from the observed creep phenomena. Therefore, all the simulations in this Subsection are conducted in isothermal conditions.

Bryant and Vadhanavikkit Tests

This Set consists of tests conducted by Bryant and Vadhanavikkit (1987), and also reported in Bazant et al. (1997a). They refer to $w/c = 0.47$ concrete, the cement used being Ordinary Portland Cement without additives. Square prisms os sides 150 mm. and length 600 mm. were subjected to an axial compressive stress of 7 MPa. for five different ages at loading, $t = 8$, 14, 28, 84 and 182 days, and sustained until about 2,000 days of age.

The material properties used for the numerical simulation are listed in Table 2. Note that only 2 Maxwell elements are used in the simulation, while the results reported in Bazant et al. (1997a) used 10 Kelvin units. It is convenient to take $\tau^1 = \infty$, so that E^1 can be considered as the *asymptotic*

Properties	B & V	Laplante OPC	Laplante HPC
w/c	0.47	0.50	0.30
s/c	0.00	0.00	0.10
ξ_∞	0.75	0.75	0.75
$k_\xi/\eta_{\xi 0}\,[1/hs]$	1.50 x 10^{10}	1.0(1.2) x 10^6	1.0(1.3) x 10^6
$\overline{\eta}$	10.0	7.5(6.0)	7.5(6.0)
$A_{\xi 0}/k_\xi$	0.3 x 10^{-6}	1.0 x 10^{-6}	1.0 x 10^{-8}
$E_a/R\,[^oK]$	6900	4000	4000
ξ_{set}	0.2	0.1	0.1
A_f	3.92	2.56	2.56
B_f	0.14	0.37	0.37
$f_\infty^-\,[MPa]$	20	47.5(35.2)	95.3(79.0)
$E_\infty\,[GPa]$	38.3	44.1(38.5)	53.8(49.4)
N	2	2	2
$E^1 : E^2$	3:1	3:1	3:1
$\tau^1\,[hs]$	∞	∞	∞
$\tau^2\,[hs]$	15	15	75(15)
$\tau_{\mu 0}\,[hs]$	600	700	1000
$c_{\mu 0}\,[1/hs]$	5.0 x 10^{-3}	6.0 x 10^{-3}	2.0 x 10^{-2}

Table 2: Material Properties for Long Term Mechanical Simulations.

elastic modulus of concrete. A relation $E^1 : E^2 = 3 : 1$ has been used for the two elastic moduli in the chain. Note also that only the values for $\tau_{\mu 0}$ and $c_{\mu 0}$ are needed for the simulation of the evolution of the micro-prestress at all ages.

Figure 7(a) shows the evolution of the elastic modulus with time; the dots represent the experimental values, and the solid line is the prediction by the model. Figure 7(b) shows the evolution of the total strain with time for loading at different ages. The overall agreement of the model predictions with the experimental results is good.

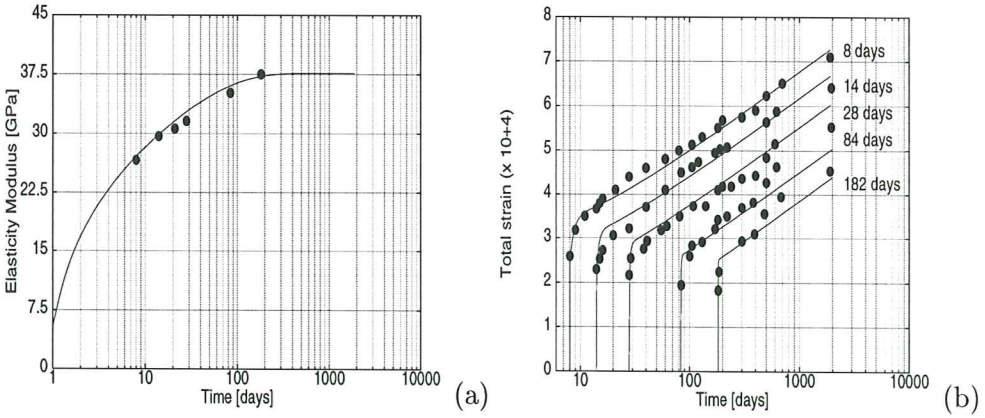

Figure 7: Long Term Mechanical Simulations. B & V Tests.

Laplante's Monotonic Tests

This Set consists of tests carried out at the Ecole Nationale des Ponts et Chaussées, Paris, France and reported in Laplante (1993). The specimens were cylinders of diameter 160 mm. and length 100 mm. Two different concrete mixes were tested. The first was a $w/c = 0.5$ Ordinary Portland Concrete without additives. The second was a $w/c = 0.3$ High Performance Concrete with silica fume and superplasticizers. The material properties used for the numerical simulation are listed in Table 2, in the columns labelled Laplante OPC and Laplante HPC, respectively. Again, only 2 Maxwell elements are used in the simulation.

Figures 8(a) and 8(b) show the comparison between the experiments and the model simulation for the evolution of the compressive strength and elastic modulus, respectively, for both mixes.

The specimens were subjected to an axial compressive stress of 30 % the compressive strength at the age of loading. Figure 8(e) shows strain versus time curves for OPC loaded at different ages, $t = 18$ hours, 1, 3, 7 and 28 days. Figure 8(f) shows strain versus time curves for HPC loaded at different ages, $t = 21$, 24 hours, 3, 7 and 28 days. Note that the experimental methodology used in these tests is different from the ones presented above. On one hand, the applied load is increased with the age at loading; on the other, tests were conducted at very early ages, less that 1 day. Nevertheless, the agreement between the experiments and the model simulation is notably good.

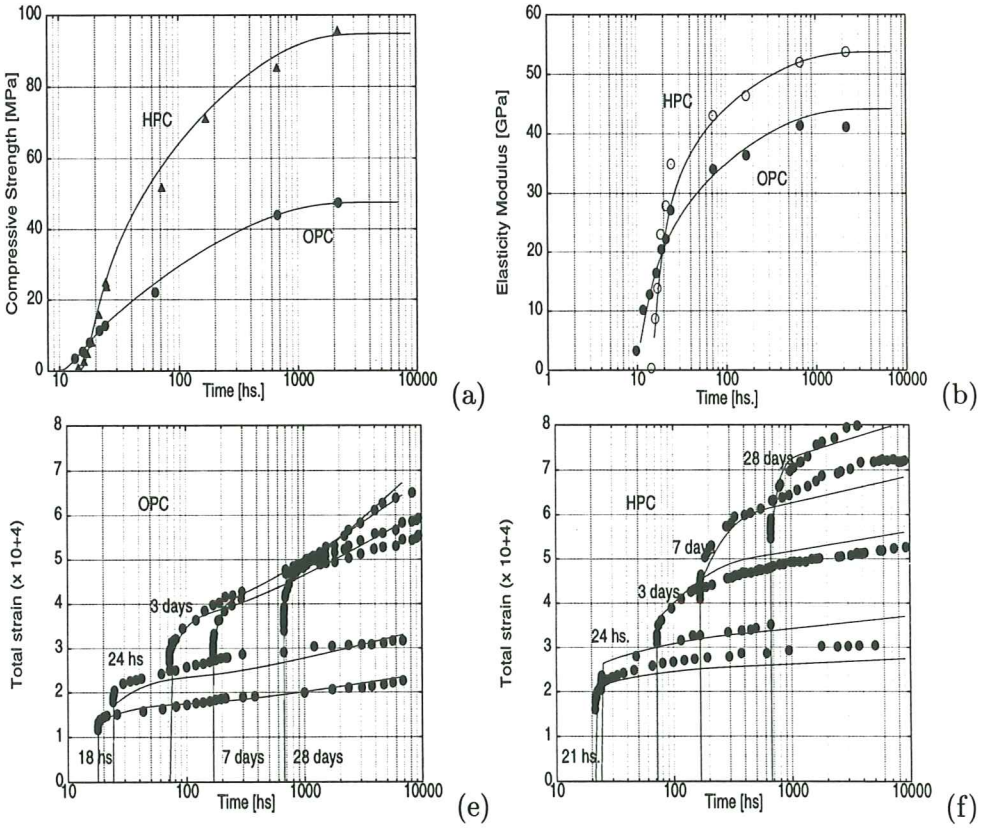

Figure 8: Monotonic Loading Simulation. Laplante's Tests.

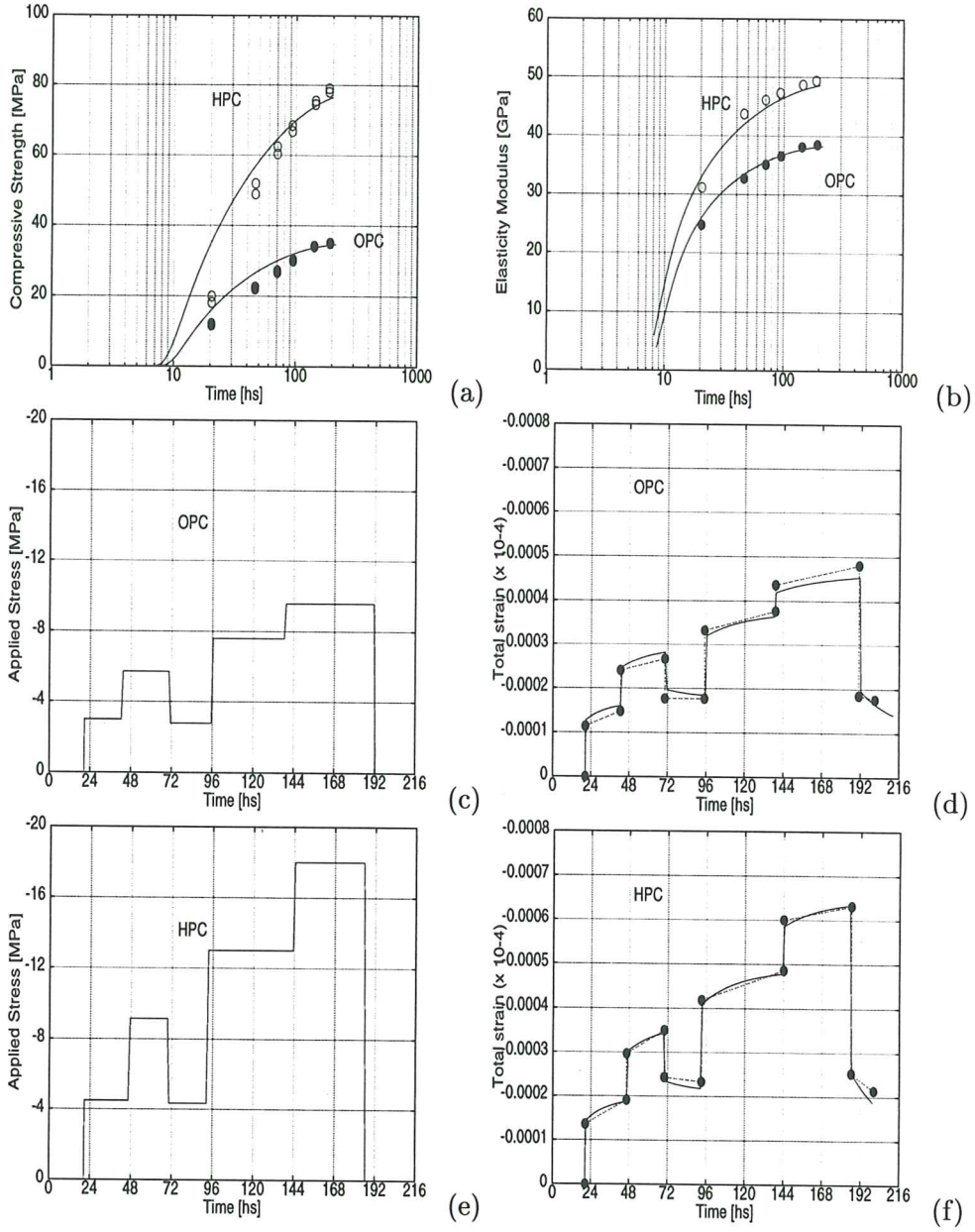

Figure 9: Cyclic Loading Simulation. Laplante's Tests.

Laplante's Cyclic Tests

This Set consists of tests carried out at the Ecole Nationale des Ponts et Chaussées, Paris, France and reported in Laplante (1993). The specimens were cylinders of diameter 300 mm. and length 120 mm. Two different concrete mixes were tested. The first was a $w/c = 0.5$ Ordinary Portland Concrete without additives. The second was a $w/c = 0.3$ High Performance Concrete with silica fume and superplastifiers.

The material properties used for the numerical simulation are listed in Table 2, in the columns labelled Laplante OPC and Laplante HPC, respectively. Note that the concret mixes used for the cyclic tests are different from the ones used for the static tests. When they differ, the values used for the numerical simulation of the cyclic tests are indicated in parenthesis. Again, only 2 Maxwell elements are used in the simulation.

Figures 9(a) and 9(b) show the comparison between the experiments and the model simulation for the evolution of the compressive strength and elastic modulus, respectively, for both mixes.

The specimens were subjected to a cyclic axial compressive stress that varied according to Figures 9(c) (for the Ordinary Portland Concrete) and 9(d) (for the High Performance Concrete). Figures 9(e) and 9(f) shows strain versus time curves for both concrete mixes. The dots and dash lines represent the experimental results, while the solid lines represent the numerical simulation. The agreement between the experiments and the model simulation is notably good. The model is capable of adequately reproducing the experimentally observed loading and unloading jumps as well as the in–between creep behaviour.

CONCLUSIONS

This paper describes a thermo-chemo-mechanical model which accounts for many of the features observed in the behaviour of concrete at early ages. A consistent thermodynamic framework is provided for these irreversible processes. Expressions for the free energy are provided from which the state equations are derived. Positive dissipation is guaranteed in all situations. The short term mechanical behaviour is based on the Continuum Damage Mechanics Theory. The novel normalized format proposed for the damage model is found to be particularly attractive, as it accomodates in a natural fashion the phenomenon of aging (with both the elastic moduli and the strength depending on the aging degree). The long term mechanical behaviour is based on the recently proposed Microprestress-Solidification Theory. The model is well suited for its implementation in a finite element devised for thermo-mechanical analysis, and its strain-driven format allows to aim to large scale computations. The capabilities and potentiality of the model are shown by performing numerical simulations of adiabatic and isothermal tests in concrete samples. The qualitative and quantitative agreement between the model results and the available experimental data is remarkably good in all situations.

APPENDIX I. REFERENCES

Bazant, Z. P. (1977). Viscoelasticity of solidifying or melting viscoelastic materials. *J. Engrg. Mech., ASCE*, 105(6):903–952.

Bazant, Z. P., editor (1988). *Mathematical modelling of creep and shrinkage of concrete.* John Wiley & Sons, New York.

Bazant, Z. P., Hauggard, A. B., and Baweja, S. (1997a). Microprestress–solidification theory for concrete creep. i: Algorith and verification. *J. Engrg. Mech., ASCE*, 123(11):1195–1201.

Bazant, Z. P., Hauggard, A. B., Prasannan, S., and Ulm, F. J. (1997b). Microprestress–solidification theory for concrete creep. i: Aging and drying effects. *J. Engrg. Mech., ASCE*, 123(11):1188–1194.

Bazant, Z. P. and Prasannan, S. (1989). Solidification theory for concrete creep. i: Formulation. *J. Engrg. Mech., ASCE*, 115(8):1691–1703.

Bryant, A. H. and Vadhanavikkit, C. (1987). Creep, shrinkage-size, and age at loading effects. *ACI Materials Journal*, pages 117–123.

Carol, I. and Bazant, Z. P. (1993). Viscoelasticity with aging caused by solidification of nonaging constituent. *J. Engrg. Mech., ASCE*, 119(11):2252–2269.

Cervera, M., Oliver, J., and Faria, R. (1995). Seismic evaluation of concrete dams via continuum damage models. *Earth. Engng. Struc. Dyn.*, 24(9):1225–1245.

Cervera, M., Oliver, J., and Galindo, M. (1992). Numerical analysis of dams with extensive cracking resulting from concrete hydration: simulation of a real case. *Dam Engineering*, 3(1):1–22.

Cervera, M., Oliver, J., and Manzoli, O. (1996). A rate-dependent isotropic damage model for the seismic evaluation of concrete dams. *Earth. Engng. Struc. Dyn.*, 25(9):987–1010.

Cervera, M., Oliver, J., and Prato, T. (1998). A thermo-chemo-mechanical model for concrete. i: Hydration and aging. *Submitted to J. Engrg. Mech., ASCE.*

Chaboche, J. L. (1988a). Continuum damage mechanics: Part i - general concepts. *J. Appl. Mech., ASME*, 55:59–64.

Chaboche, J. L. (1988b). Continuum damage mechanics: Part ii - damage growth. *J. Appl. Mech., ASME*, 55:65–72.

Faria, R., Oliver, J., and Cervera, M. (1998). A strain-based plastic viscous-damage model for massive concrete structures. *Int. J. Solids and Structures*, 35(14):1533–1558.

Galindo, M. (1993). *Una metodología para el análisis numérico del comportamiento resistente no lineal de presas de hormigón bajo cargas estáticas y dinámicas (in Spanish).* PhD thesis, Technical University of Catalonia.

Kachanov, L. M. (1958). Time of rupture process under creep conditions. *Izvestia Akademii Nauk, Otd Tech Nauk*, 8:26–31.

Khan, A. A., Cook, W. D., and Mitchell, D. (1995). Early age compressive stress-strain properties of low-medium, and high-strength concretes. *ACI Materials Journal*, 92(6):617–624.

Khan, A. A., Cook, W. D., and Mitchell, D. (1998). Thermal properties and transient thermal analysis of structural members during hydration. *ACI Materials Journal*, 95(3):293–303.

Laplante, P. (1993). *Mechanical properties of hardening concrete: A comparative analysis of classical and high strength concretes (in French).* PhD thesis, Ecole Nationale des Ponts et Chaussées, Paris, France.

Lemaitre, J. (1984). How to use damage mechanics. *Nuclear Engineeing Design*, 80:233–245.

Lemaitre, J. and Chaboche, J. L. (1978). Aspects phénoménologiques de la rupture par endommagement (in french). *J. Méc. Appl.*, 2:317–365.

Mazars, J. and Pijaudier-Cabot, G. (1989). Continuum damage theory: Application to concrete. *J. Engrg. Mech., ASCE*, 115:345–365.

Oliver, J. (1989). A consistent characteristic length for smeared cracking models. *Int. J. Num. Meth. Engng.*, 28:461–474.

Prato, T., Cervera, M., and Oliver, J. (1997). *Simulación Numérica del Proceso de Hidratación del Hormigón (in Spanish).* Publicación CIMNE N. 14.

Simó, J. C. and Ju, J. W. (1987a). Strain- and stress-based continuum damage models - i. formulation. *Int. J. Solids and Structures*, 23(7):821–840.

Simó, J. C. and Ju, J. W. (1987b). Strain- and stress-based continuum damage models - ii. computattional aspects. *Int. J. Solids and Structures*, 23(7):841–869.

APPENDIX II. NOTATION

The following symbols are used in this paper:

A_d, B_d = Material properties for hard-softening behaviour;
A_ξ, $A_{\xi 0}$ = Chemical affinity, Initial chemical affinity;
$\widetilde{A}_\xi$ = Normalized chemical affinity;
C = Heat capacity per unit volume;
$\boldsymbol{C}^\pm$ = Tensile/compressive metric (fourth order) tensors;
$\boldsymbol{D}, \overline{\boldsymbol{D}}$ = Constitutive (fourth order) tensor; Normalized *idem*
$d^\pm$ = Compressive/tensile damage;
$\mathcal{D}_{chem}, \mathcal{D}_{mech}$ = Chemical dissipation, Mechanical dissipation;
E, E_∞ = Elastic modulus, Final elastic modulus;
E^i = Elastic Modulus for Maxwell element i;
$f^\pm, f^\pm_\infty$ = Tensile/compressive strength, Final values;
$f^\pm_e$ = Elastic limit in uniaxial tests (tension/compression);
$\hat{g}^\pm, g^\pm$ = Damage criteria, Normalized damage criteria;
$G^\pm_f$ = Tensile/compressive fracture energy;
K, G = Bulk and shear moduli;
l^* = Characteristic length;
L = Thermo-mechanical contribution to the free energy;
$\boldsymbol{p}_j$ = Unit vector associated with principal direction j;
Q_ξ = Latent heat per unit of hydration degree;
$\hat{r}^\pm, r^\pm$ = Damage tensile/compress. thresholds,
Normalized damage tensile/compress. thres.;
$r^\pm_e$ = Normalized elastic tensile/compress. thresholds;
$r^\pm_p$ = Normalized peak values for tensile/compress. thres.;
S = Entropy;
s/c = Silica fume/cement mass ratio;
T, T_0 = Temperature, Initial temperature;

T_∞^{ad} = Final temperature reached in an adiabatic test;
T_{ref} = Reference temperature;
V = Thermal contribution to the free energy;
v = Solidified fraction;
W, W_e = Mechanical contribution to the free energy, Elastic mech. contribution to the free energy;
$W^{\pm}, W_e^{\pm}$ = Tensile/compress. mech. part of the free energy, Elastic tens./compr. mech. part of the free energy;
$W_e^{i\pm}$ = Elastic tensile/compress. mech. contribution to the free energy of a Maxwell element;
w/c = Water/cement mass ratio;
α_T, α_ξ = Thermal and chemical expansion coefficients;
$\boldsymbol{\varepsilon}, \boldsymbol{\varepsilon}_e$ = Strain tensor, Elastic strain tensor;
$\boldsymbol{\varepsilon}_e^i, \boldsymbol{\varepsilon}^i$ = Elastic, Viscous strain tensor for Maxwell element i;
$\boldsymbol{\varepsilon}_T, \boldsymbol{\varepsilon}_\xi$ = Thermal strain tensor, Chemical strain tensor;
$\eta_\mu, \eta_{\mu 0}$ = Viscosity of the flow term; Initial viscosity;
$\gamma^{\pm}$ = Parameter to define the metric tensors;
κ = Aging degree;
λ_E = Elastic modulus aging function;
$\lambda_f^{\pm}$ = Tensile/compressive strength aging functions;
$\lambda_e^{\pm}$ = Elastic threshold aging functions;
μ = Normalized micro-prestress;
ν = Poisson's ratio;
Ψ = Free energy;
$\rho^{\pm}$ = Ratio biaxial/uniaxial strengths;
$\boldsymbol{\sigma}, \overline{\boldsymbol{\sigma}}$ = Stress tensor, Effective stress tensor;
$\bar{\sigma}_j$ = Principal effective stress value j;
$\sigma_\mu, \sigma_{\mu 0}$ = Micro-prestress; Initial micro-prestress;
τ^i = Relaxation time for Maxwell element i;
$\tau_\mu, \tau_{\mu 0}$ = Relaxation time associated to flow term, Initial value;
ξ, ξ_∞ = Hydration degree, Final hydration degree;
$\mathbf{1}$ = Unit (second order) tensor;
$\boldsymbol{I}$ = Unit (fourth order) tensor;
$\dot{(\,)}$ = Time derivative or rate;
$(\,) \otimes (\,)$ = Tensorial product;
$(\,) : (\,)$ = Doubly contracted tensorial product; and
$< >$ = Macaulay brackets.